AIMS Energy, 11(6): 1153–1178.
DOI: 10.3934/energy.2023053
Received: 01 August 2023
Revised: 24 October 2023
Accepted: 01 November 2023
Published: 17 November 2023

http://www.aimspress.com/journal/ energy

Research article

Mathematical modeling of a binary ORC operated with solar collectors. Case study—Ecuador

Daniel Chuquin-Vasco[1,*], Cristina Calderón-Tapia[2], Nelson Chuquin-Vasco[3], María Núñez-Moreno[4], Diana Aguirre-Ruiz[5] and Vanesa G. Lo-Iacono-Ferreira[6]

[1] Escuela Superior Politécnica de Chimborazo (ESPOCH), Chemical Engineering Career, Safety, Environment and Engineering Research Group (GISAI), Riobamba, Ecuador
[2] Escuela Superior Politécnica de Chimborazo (ESPOCH), Environmental Engineering Career, Riobamba, Ecuador
[3] Escuela Superior Politécnica de Chimborazo (ESPOCH), Mechanical Engineering Career, Safety, Environment and Engineering Research Group (GISAI), Riobamba, Ecuador
[4] Escuela Superior Politécnica de Chimborazo (ESPOCH), Environmental Engineering Career, Riobamba, Ecuador
[5] SOLMA, Advanced Mechanical Solutions, Mechanical Engineering and Construction Services
[6] Project Management, Innovation and Sustainability Research Center (PRINS), Alcoy Campus, Universitat Politècnica de València, Alcoy, Spain

* **Correspondence:** Email: daniel.chuquin@espoch.edu.ec; Tel: +593998163018.

Abstract: The present study is significant because it can contribute to developing sustainable energy strategies and expanding knowledge about renewable energies in Ecuador, specifically by modeling two modules: the thermal module (parabolic solar collectors and energy storage tank) and the Organic Rankine Cycle (ORC) module. The objective was to determine a region in Ecuador where the thermal module exhibits the highest efficiency for solar collectors. Subsequently, a detailed analysis of the ORC module was conducted, considering the working fluid, boiling temperature, condensation temperature, pinch point temperature, solar collector area, and the collector area-to-energy storage volume ratio (*Ac/V*). Finally, an economic analysis was performed based on the Net Present Value (NPV), Internal Rate of Return (IRR), and payback period of implementing this type of system. After conducting all the respective analyses in the thermal module, while considering the yearly average meteorological data of ten years (2012–2022), it was determined that due to its meteorological conditions, ambient temperature (14.7 °C) and solar beam radiation (184.5 W/m^2), the efficiency of the collectors

in the Andean region of Ecuador is higher. This efficiency is further enhanced by using Therminol VP-1 as the thermal fluid, as it possesses better thermodynamic properties than the other fluids analyzed. Similarly, the ORC module analysis results determined that cyclohexane is the working fluid for the ORC, thereby leading to a higher ORC efficiency (25%) and overall system efficiency (20%). Finally, the system was optimized to maximize the IRR and minimize the Ac/V of the collector for a nominal power of 92 kW. As a result, the optimal operating conditions of the system include a solar collector area of 1600 m², an energy storage tank volume of 54 m³, an electricity production of 23757 MW/year, a total system efficiency of 22%, an IRR of 15.65% and a payback period of 9.81 years.

Keywords: solar collectors; working fluid; ORC; thermal module; energy

Nomenclature: Ac: Collecting area (m^2); Ast: Storage tank area (m^2); C_p: Specific heat capacity (kJ/kg); Co: Capital cost (€); DSt: Storage tank diameter (m); Eel: Energy electric (J); Egrid: Energy solar (J); Esolar: Energy given to the grid (J); Gb: Solar beam radiation (W/m^2); h: Enthalpy (J/kg); K: Specific cost (€/kWh); L: Longitude (m); M: Molecular weight (kg/mol); M: Mass flow rate (kg/s); η: Efficiency; Q: Heat rate (W); r: Discount factor (%); T: Temperature (°C); UL: Heat losses coefficient of tank (W/(m^2·K)); V: Volume (m^3); W: Specific work pump (kJ/kg)

Subscripts: amb: Ambient; c: Collector; el: Electric; grid: Energy given to the grid; in: Inlet; L: Thermal oil; Loss: Thermal loss; mg: Mechanical & generator; mot: Motor; ORC: Organic Rankine Cycle; out: Outlet; O&M: Operation and maintenance; Pump: Working fluid pump; res: Residual; sat: Saturation; solar: Solar energy; u: Useful; st: Storage tank; w: Waste

1. Introduction

As the population grows, the need for electrical energy increases. The production from non-renewable sources, such as the burning of fossil fuels, which represents a serious environmental impact, is often chosen to meet the demand [1]. From this perspective, due to its geographical location, Ecuador began to utilize solar energy as an alternative to hydroelectric power plants, which currently covers 76.65% of the total electricity demand in the country, with only 0.11% corresponding to photovoltaic energy [2]. The advantage lies in Ecuador's location on the equator, where direct solar radiation is perpendicular throughout the year, varying only based on the meteorological conditions of each region within Ecuador (Coast, Andean, Amazon, and Galapagos Island). In line with the use of solar energy, according to the National Energy Efficiency Plan (2016–2035), the main and current objective is to reduce energy consumption per unit of physical production in the industrial subsectors by employing energy cogeneration systems, which can be combined with solar collectors to increase the energy efficiency of the system. Additionally, hybrid nanofluids offer a promising solution for solar steam generation by significantly improving solar energy utilization and evaporation efficiency. In this context, their excellent stability, high solar irradiation absorption capacity, and increased solar-thermal conversion efficiency at higher mass concentrations further emphasize their potential [3,4].

With the current implementation of these techniques, it is estimated that companies can reduce their energy consumption by 29.9 Mtoe (Million of tonne of oil equivalent) by 2035. Currently, "only three sugar mills supply electrical energy through cogeneration, with a total capacity of 136.4 MW" [5].

1.1. Organic Rankine Cycle (ORC)

The global energy demand has increased because of overpopulation, which compels governments to seek environmentally friendly alternatives for electricity generation through renewable energy sources and/or the utilization of waste heat from industrial processes. Organic Rankine Cycle (ORC) systems are power systems that have simple configurations and the ability to operate at low temperatures with high efficiencies by using organic substances as working fluids, which have low boiling points [6].

Review articles such as those presented by Bao and Zhao [7], Lecompte et al. [8], and Vélez et al. [9] have provided an overview of the cycles, selection of working fluids, and the system's main components. However, most existing studies have solely focused on technical difficulties related to the heat source for specific case studies. The heat source is one of the most important aspects during the design and construction of an ORC, as the working conditions and thermodynamic efficiency of the cycle are determined by the heat source used. The main heat sources used in ORC systems come from waste heat in industrial processes, internal combustion engines, gas turbines, renewable energies (solar, geothermal, biomass), and the key parameters considered for their selection are temperature, capacity, thermodynamic behavior, and cost [10].

The most common method of generating electricity from solar energy is through the application of the basic Rankine cycle. However, when the temperatures of the heat source are low (i.e., around 300 °C), the ORC is preferred [11]. Around this temperature, various working fluids are used, such as Octamethyltrisiloxane (MDM), Hexamethyldisiloxane (MM), isopentane, and cyclohexane, among others, due to their thermal characteristics. The lower critical point and the positive slope formed in the temperature vs entropy (T-s) diagram are factors that determine the suitability of the selected working fluid [12]. Within the temperature range of 150–200 °C, isopentane and isobutane are generally used as working fluids [13,14]. Delgado-Torres et al. [13] conducted studies to determine the performance of different solar collectors (PTC—Parabolic Trough Collectors, ETC—Evacuated Tube Collectors, FPC—Flat Plate Collectors) on the thermal efficiency of an ORC in desalination systems for electricity production (0.5 MW) using MM and R245fa as working fluids. They found that the use of parabolic trough collectors led to a higher performance.

1.2. Thermodynamic analysis of the ORC

ORCs operate with high molecular weight organic fluids that have different critical thermodynamic properties compared to water, and they are characterized by enhancing heat recovery and cycle efficiency [15,16]. Figure 1 shows the main components of a basic ORC and the T-s diagram, which represents the four ideal processes of the cycle. The basic ORC consists of a pump that raises the working fluid pressure and transports it to the evaporator (Point 1). In the evaporator, the working fluid is heated to either its saturation point or superheated vapor state (Point 2). Then, the fluid expands in the turbine, produces mechanical work (Point 3) and is converted into electrical energy through a generator. The superheated fluid is condensed back into a saturated liquid (Point 4). Finally, the pressure is raised by the pump, thus closing the thermodynamic cycle. The dissipated and supplied heat represent a finite thermal reservoir and are represented by Points (7,8) and Points (5,6) in Figure 1(a).

The selection of the working fluid is crucial in ORC processes and depends on the specific application for which it will be designed [17]. The ORC could work with either constantly saturated

or superheated vapor. Superheating at high temperatures to prevent vapor carryover of liquid droplets is not necessary because, unlike water, the expansion of most fluids ends in the superheated vapor region. Superheating improves the cycle efficiency; however, due to the low heat transfer coefficients in the heat exchangers, large and expensive heat exchangers are required [18]. The technical criteria for selecting the type of fluid include the thermodynamic cycle efficiency, net power produced, return on investment, and net power produced per unit heat transfer area, while the thermodynamic parameters taken into consideration include the boiling critical pressure and temperature, condensation critical pressure and temperature, latent heats, low freezing point, low enthalpy of vaporization, and low environmental impact [16].

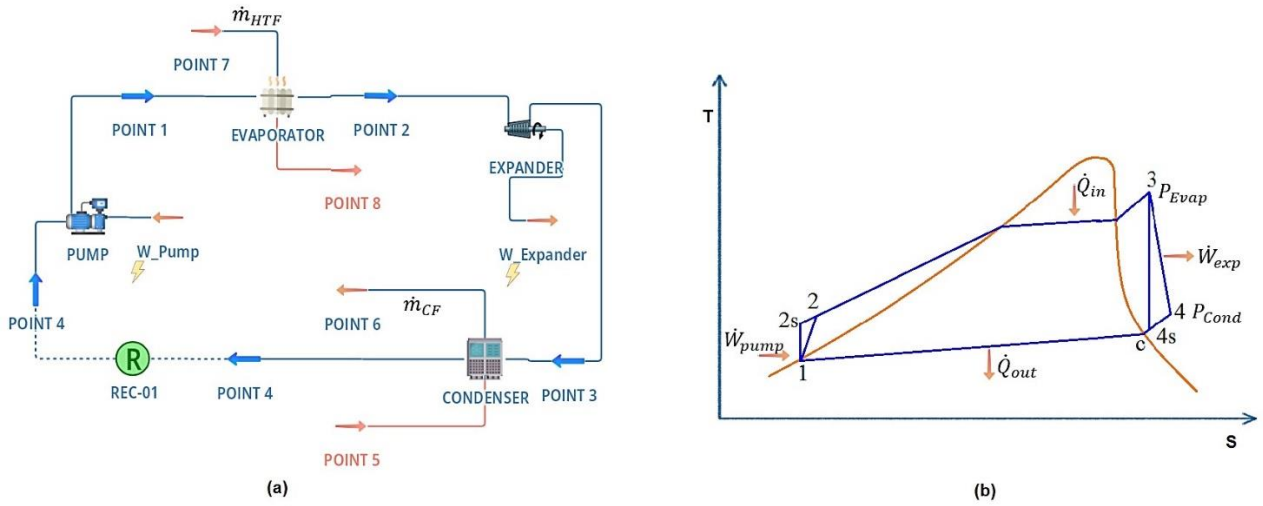

Figure 1. (a) Main components of an ORC, (b) T-s diagram of an ORC.

1.3. Heat source in ORCs

Based on their configuration, power, and heat source temperature, ORC's have the ability to harness different types of available energy, such as industrial waste heat, geothermal, solar, exhaust gases, and nuclear energy [9]. The categorization of heat sources is important for optimizing the thermodynamic cycle and selecting the working fluid. Table 1 provides detailed characteristics of the typical heat sources used in ORC's.

Generally, solar collectors operated at high temperatures provide good efficiencies to the ORC. However, this leads to a decrease in the collector's efficiency, and the implementation costs of solar panels increase. For this reason, each system is designed with an optimal design temperature [19]. Energy storage in solar collectors depends on the fluctuation in solar radiation levels. Several studies have employed dynamic models to evaluate the effects of radiation on electricity generation based on meteorological conditions [20–22]. In ORC systems operated with solar collectors, radiation is stored as energy in reservoirs installed between the collectors and the ORC to maintain system efficiency. Typically, these systems have three modes of operation: solar mode during periods of low insolation, solar mode with energy storage during periods of high insolation, and the release of stored energy at night [23].

Table 1. Heat source characteristics.

Heat source	Temperature	Medium	Capacity	System cost	References
Industrial	80–500 ℃	Water, oil, or steam	0.125–3 MW	$1800–$5500 /kW	[24,25]
Residual heat	80–100 ℃ (Cooling system) 400–900 ℃ (Exhaust gases)	Water or oil with other gases	0.095–6.5 MW	-	[26–28]
Geothermal	80–180 ℃	Brine water	0.6–27 MW	$1500–$5000	[29,30]
Solar collector	<300 ℃	Water or oil	<30 MW	$6000–$7500 /kW	[31]
Biomass	Aprox. 300 ℃	Oil	100–1500 kW	$2000/kW (medium scale) $12000/kW (big scale)	[32–34]

Ecuador's strategic advantage for solar energy projects lies in its consistent tropical climate, which is further characterized by minimal annual variations. This stability ensures reliable solar energy generation, thus making it an ideal location for sustainable solar projects [35].

This work stands as a pioneering endeavor within the Ecuadorian context. To date, no similar study or proposal of this nature has been conducted in the region. The comprehensive approach makes this research not only particularly innovative, but also considers the integration of waste heat from environmentally polluting industries by harnessing solar collectors for sustainable energy generation. Consequently, our project promises to usher in a transformative era of reduced environmental footprints and enhanced sustainability in Ecuador's energy landscape.

2. Materials and methods

In this work, an ORC system will be modeled using solar collectors (thermal module) and waste heat as the heat source. The model was developed to determine the optimal design parameters that maximize the thermal efficiency of the ORC while minimizing the solar energy capture area.

Figure 2 details the methodological scheme for the development and evaluation of the model. Initially, a thermodynamic analysis of the thermal oil used in the thermal module and the working fluids of the ORC Module was conducted based on the operating conditions imposed by the system. Subsequently, an energy evaluation was performed to determine an optimal solution by maximizing the IRR. The parameters subject to optimization were the solar panel capture area, the volume of the energy storage tank, and the system installation costs.

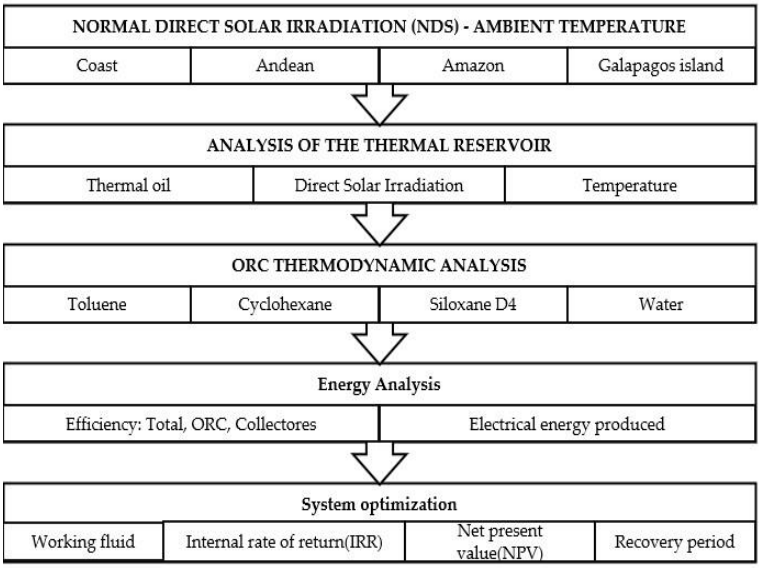

Figure 2. Methodology for system modeling ORC.

2.1. System description

Figure 3 shows the diagram of the modeled system, which consists of 2 modules: The thermal module and the ORC module (with a recuperator).

The thermal module is composed of a set of solar collectors operated with thermal oil and an energy storage tank, which together have the capacity to transfer heat to the ORC module through the heat exchanger. The collectors used in the modeling were similar to the Eurotrough ET-150, which has a tracking control (clock + solar sensor, <2 rad) and which provides better efficiencies at a lower system cost [36,37].

Meanwhile, the ORC module is composed of five components (a pump, a heat exchanger, a turbine, a recuperator, and a condenser) in which four processes take place. In processes 1 and 2, a compression process occurs, where the fluid, initially in a low-pressure saturated liquid state, enters the pump to reach the maximum cycle pressure. In processes (2,3) and processes (5,6) the fluid is internally heated by the exchange of heat (i.e., via the recuperator) with the saturated vapor from the turbine to increase the overall energy efficiency of the cycle. In processes 3 and 4, heat transfer (i.e., via the heat exchanger) occurs between the thermal module's thermal oil and the ORC's working fluid, resulting in superheated vapor at Point 4. In processes 4 and 5, the superheated vapor expands in the turbine to the minimum cycle pressure, thereby transforming the working fluid into saturated vapor (Point 5). Finally, in processes 6 to 1, the saturated vapor is converted back into saturated liquid in the condenser (i.e., heat rejection) to initiate the cycle again.

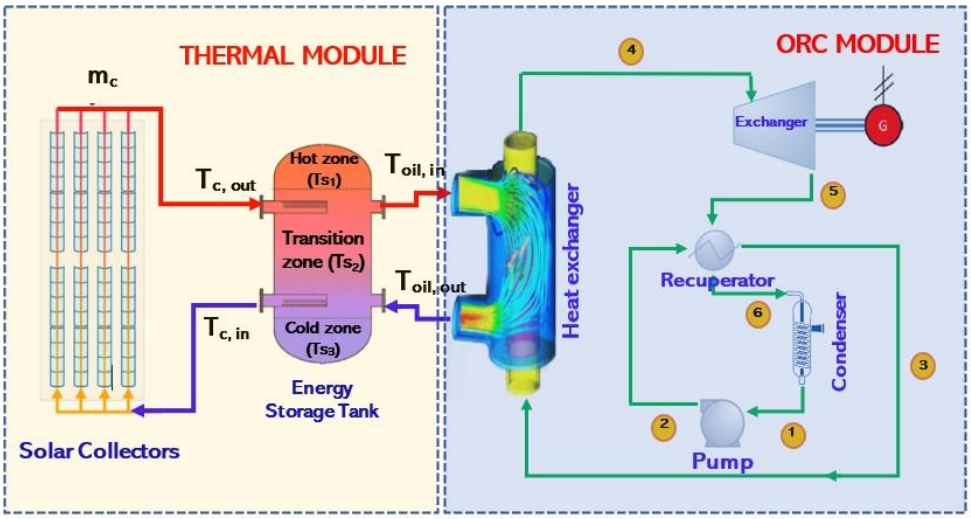

Figure 3. Schematic representation of the model.

2.2. Modeling parameters

The meteorological data used in the modeling process were obtained from the National Renewable Energy Laboratory (NREL), which recorded the average temperatures and solar radiation in 30-minute measurement intervals (Time series: 2012–2022). Given that the typical temperature varies throughout the year for various regions, the analysis considered four regions of Ecuador: Coast, Andean, Amazon, and Galapagos Islands. Figure 4 shows the ambient temperature (T_{amb}) for each of the regions in Ecuador, while Figure 5 details the solar irradiation values received by the collector depending on the region where it is located. It is important to note that only the direct normal irradiation can be used by the parabolic trough collectors since they only absorb a specific solar image. Table 2 provides detailed conditions assumed for the system modeling. These values have been reasonably selected based on real operating conditions and have been tested in preliminary studies [38].

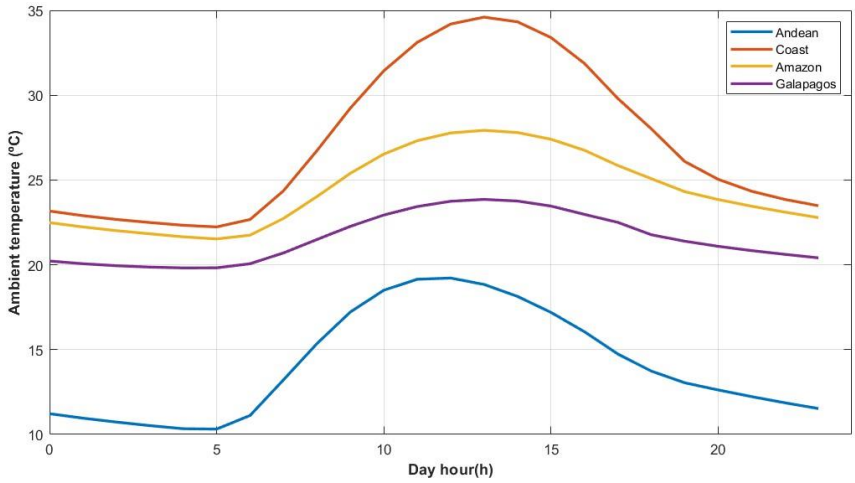

Figure 4. Average ambient temperature (30-minute scale; time series: 2012–2022)—Ecuador regions.

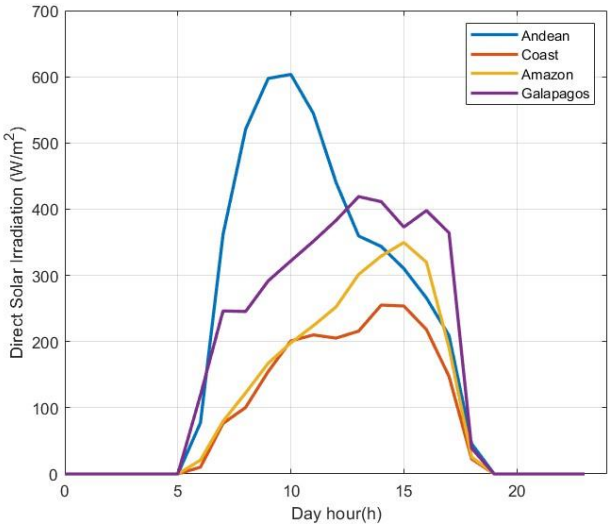

Figure 5. Average direct solar radiation ambient temperature (30-minute scale; time series: 2012–2022)—Ecuador regions.

Table 2. Operating parameters of the thermal module and the ORC.

Parameter	Simbology	Value	Reference
Collector volume/area ratio	V/*A*c	8 < V/*A*c < 100	[39]
Maximum temperature	$T_{oil,max}$	300 ℃	[19]
ΔT of thermal oil	ΔT_{oil}	50 ℃	[37]
Thermal tank heat loss coefficient	uL	1 W/(m^2·K)	[37]
Isentropic turbine efficiency	$\eta_{is,T}$	85%	[40]
Turbine pressure ratio	$\Pi_{T,max}$	60	[37]
Isentropic pump efficiency	$\eta_{is,b}$	70%	[40]
Engine efficiency	η_{motor}	70%	[37]
Generator and machine efficiency	η_{mg}	97%	[41]
Recovery efficiency	η_{Re}	60%	[40]
Condensation temperature	T_{cond}	60 ℃	[37]
ΔT in the regenerator	ΔT_{sh}	10 ℃	[42]
Pinch point	*PP*	>5 ℃	[43]
Pressure relationship	*P*max/*P*crit	0.9	[41]

2.3. Mathematical model

A sequential list of equations (Eqs 1–17) employed during model development can be found in Table 3. These equations served to model both the thermal module and the ORC system. The solutions to these equations were derived using multistep implicit methods, specifically the Adams-Bashforth method for the initial value problems, in conjunction with the double Newton method. The thermodynamic properties required for ORC calculations were computed using the EES-Demo software. The entire model was constructed using MATLAB R2018a, thereby facilitating a comprehensive analysis of thermodynamic properties, with a primary focus on assessing the collector efficiency, the thermodynamic cycle efficiency, and the total electrical energy production. Furthermore,

optimization procedures were executed using nonlinear reduced generalized gradient algorithms, with the net present value (NPV) serving as the objective function. The financial parameters of the present study are included in Table 4.

Table 3. Equations used for system modeling.

Module	Parameter	Equation		Reference
Thermal	Available solar irradiation	$Q_{\text{solar}} = A_{\text{c}} * G_{\text{b}}$	(1)	[44]
	Solar collector efficiency (*Eurotrough ET-150)*	$n_c = 0.7408 - 0.0432 * \left(\frac{T_{in}-T_{am}}{G_b}\right) - 5.03 * 10^{-4} * G_b * \left(\frac{T_{in}-T_{am}}{G_b}\right)^2$	(2)	[36]
		$n_{\text{c}} = \frac{Q_{\text{u}}}{Q_{\text{solar}}}$	(3)	
	Absorbed useful energy	$Q_{\text{u}} = \text{m} * \ c_p * (T_{\text{out}} - T_{\text{in}})$	(4)	[44]
	Evolution of temperature in the hot zone (Energy storage tank)	$Mc_p \frac{\partial T_{\text{St1}}}{\partial \text{t}} = \dot{\text{m}}_{\text{c}} * c_p * (T_{\text{out}} - T_{\text{St1}}) + \dot{\text{m}}_{\text{oil}} * c_p * (T_{\text{St2}} - T_{\text{St1}}) - U_{\text{L}} * A_{\text{St1}} * (T_{\text{St1}} - T_{\text{amb}})$	(5)	[23]
	Evolution of temperature in the transition zone (Energy storage tank)	$Mc_p \frac{\partial T_{\text{St2}}}{\partial \text{t}} = \dot{\text{m}}_{\text{c}} * c_p * (T_{\text{St1}} - T_{\text{St2}}) + \dot{\text{m}}_{\text{oil}} * c_p * (T_{\text{St3}} - T_{\text{St2}}) - U_{\text{L}} * A_{\text{St2}} * (T_{\text{St2}} - T_{\text{amb}})$	(6)	[45]
	Evolution of temperature in the cold zone (Energy storage tank)	$Mc_p \frac{\partial T_{\text{St3}}}{\partial \text{t}} = \dot{\text{m}}_{\text{c}} * c_p * (T_{\text{St2}} - T_{\text{St3}}) + \dot{\text{m}}_{\text{oil}} * c_p * \left(T_{\text{oil,out}} - T_{\text{St3}}\right) - U_{\text{L}} * A_{\text{St3}} * (T_{\text{St3}} - T_{\text{amb}})\text{b}$	(7)	
	Area of the energy storage tank	$A_{\text{St1}} = \frac{\pi D_{\text{St}}^2}{4} + \frac{\pi D_{\text{St}} * L_{\text{St}}}{3}$	(8)	
		$A_{\text{St2}} = \frac{\pi D_{\text{St}} * L_{\text{St}}}{3}$	(9)	
		$A_{\text{St3}} = \frac{\pi D_{\text{St}}^2}{4} + \frac{\pi D_{\text{St}} * L_{\text{St}}}{3}$	(10)	
ORC	ORC net work	$W_{\text{net}} = \eta_{\text{mg}} * \eta_{\text{orc}} * (h_4 - h_5) - \frac{m_{\text{orc}} * w_{\text{pump}}}{\eta_{\text{mot}}}$	(11)	[46,47]
	Net heat of the ORC	$Q_{\text{net}} = m_{\text{oil}} * cp_{\text{oil}} * \Delta T_{\text{oil}}$	(12)	[44]
	ORC efficiency	$\eta_{\text{orc}} = \frac{W_{\text{net}}}{Q_{\text{net}}}$	(13)	[46,47]

Continued on next page

Module	Parameter	Equation		Reference
Thermal-ORC	Total system efficiency	$\eta_{\mathrm{tot}} = \frac{E_{\mathrm{el}}}{E_{\mathrm{solar}}}$	(14)	[23,45]
		$\eta_{\mathrm{tot}} = \eta_{\mathrm{c}} * \eta_{\mathrm{orc}} * \eta_{\mathrm{loss}}$	(15)	
	Net present value (NPV)	$NPV = -C_{\mathrm{o}} + \sum_{\mathrm{k=1}}^{\mathrm{N}} \frac{E_{\mathrm{grid}} * K_{\mathrm{el}} - K_{\mathrm{O\&M}} * C_{\mathrm{o}}}{(1+\mathrm{r})^K}$	(16)	[37]
	Capital cost ($)	$C_{\mathrm{o}} = K_{st} * V_{st} + K_{orc} * W_{\mathrm{net}} + K_c * A_c$	(17)	[37]

Table 4. Financial parameters of the analysis.

Parameter	*Value*
K_{st}	2223 \$/m^3
N	25
r (%)	5
K_{orc}	2667.6 \$/kW
K_{c}	340 \$/m^2
$K_{O\&H}$ *(%)*	2

3. Results and discussion

3.1. Model validation

To validate the model, the established operating conditions in Table 2 were employed. The results were compared with the work conducted by Tzivanidis et al. [12]. As shown in Table 5, the calculated percentage errors (%E) are below 3%, indicating the reliability of the modeled process.

Table 5. Model validation.

Working fluid	Parameter	Tzivanidis et al. [12]	Developed model	Error (%)
Cyclohexane	T oil input ($T_{\mathrm{oil,in}}$)	295.6 ℃	292.35 ℃	0.82%
	Solar collector efficiency (η_{c})	61.44%	63.22%	2.96%
	ORC efficiency (η_{orc})	25.36%	24.80%	2.91%

3.2. Solar collectors analysis

Three analyses were conducted based on the performance of the solar collector, considering four thermal oils (Therminol VP1, Solar Salt, Hitec, Hitec XL) since their thermodynamic properties are an important factor in determining the maximum thermal efficiency of the collectors. Additionally, the environmental conditions (direct solar radiation and ambient temperature) of the four regions of Ecuador were considered.

3.2.1. Required mass flow

Figure 6 represents the variation of the flow vs. the heat capacity of the thermal oil, where the green dots represent the heat capacity at a constant pressure of the thermal oils analyzed in the model. As shown in Figure 6, the required mass flow rate varies depending on the specific heat capacity (C_p) of the thermal oil used. The higher the C_p delivered by the oil, the lower the mass flow rate required to achieve the same power output of the ORC cycle and the solar collector efficiency. Using oil with superior thermodynamic properties reduces the required investment in the thermal module. Table 6 provides details of the analyzed thermal oils' characteristics and the required mass flow rate to produce 38 kW (maximum net power, minimizing the $Ac/v = 10^{-1}\ m$ based on [48]) with a collector efficiency of 50.75%, while maintaining the ambient temperature at 14.07 °C and the direct radiation at 194.98 W/m² (Andean Region weather conditions), using cyclohexane as the working fluid in the ORC. Based on the analysis, Therminol VP1 requires the lowest mass flow rate to achieve the same efficiency.

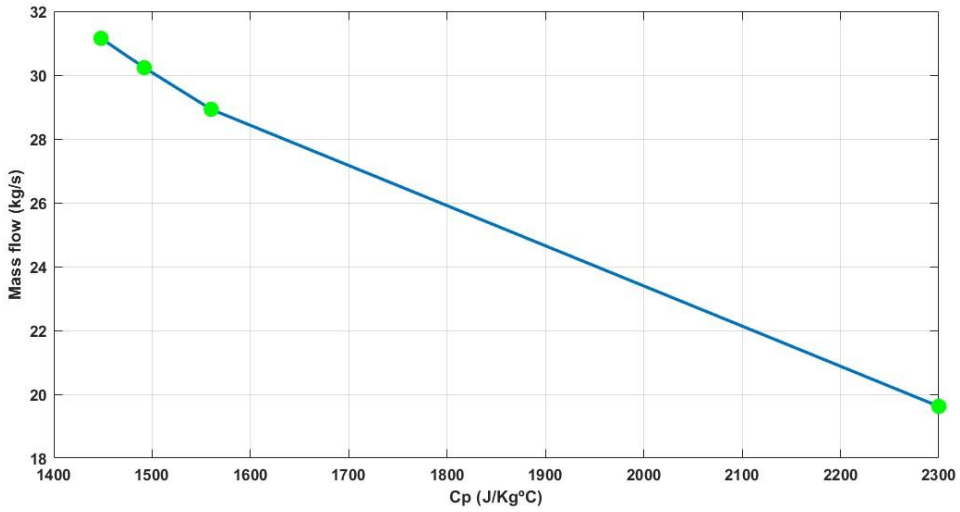

Figure 6. Mass flow rate required based on the thermal oil's specific heat capacity.

Table 6. Mass flow rate required based on the C_p.

Thermal oil	C_p (kJ/(kg·°C))	Mass flow required (kg/s)	$T_{in} = T_{s3}$ (°C)	T_{out} (°C)
Therminol VP1	2300	19.62		
Hitec	1560	28.92		
Molten salts	1492	30.23	259.81	309.96
Hitec XL	1448	31.15		

3.2.2. Collector performance based on the heat capacity of the oil

The collector's efficiency was determined based on the thermal oil's specific heat capacity, thus maintaining a mass flow rate of 19.62 kg/s and a temperature differential between the collector's inlet and outlet of 50 °C. As shown in Table 7, the higher the specific heat capacity (C_p) of the thermal oil, the greater the efficiency of the solar collector, since efficiency is directly proportional to the heat

generated by the solar collector. The Therminol VP1 oil provides improved operability of the solar collector, thereby achieving an approximate efficiency of 56%. This verifies what was established by [49], which determined that Therminol VP1 is the most suitable oil for the operation of solar collectors, since its stability ranges from 12 to 400 °C, and its thermodynamic efficiency is better compared to other working fluids such as molten salts and steam.

Table 7. Mass flow rate required based on the C_p.

Thermal oil	C_p (kJ/(kg·°C))	η_c
Therminol VP1	2300	55.40%
Hitec	1560	37.58%
Molten salts	1492	35.94%
Hitec XL	1448	34.98%

3.2.3. Collector performance as a function of the amount of direct solar irradiation

The collector's efficiency was calculated based on the amount of direct solar irradiation received by the collector and the ambient temperature in each of the regions of Ecuador. For this analysis, the average ambient temperature and the direct solar radiation from a 10-year time series were used. The Coast region recorded the highest T_{amb} (27 °C) and the Andean region had the lowest T_{amb} (14 °C). However, the highest levels of solar radiation were observed in the Andean region (194.98 W/m^2). As shown in Table 8, the collector efficiency is higher in the Andean region due to its higher radiation levels compared to the other regions. The ideal conditions would be that both T_{amb} and G_b are higher; however, due to the topographical, hydrographic and climatological conditions in Ecuador, it is challenging for these two factors to increase proportionally. In Figure 7, the green dots illustrate the relationship between the collector efficiency and both the ambient temperature and the solar radiation within the four regions of Ecuador (Coast, Andean, Amazon, and Galapagos Island).

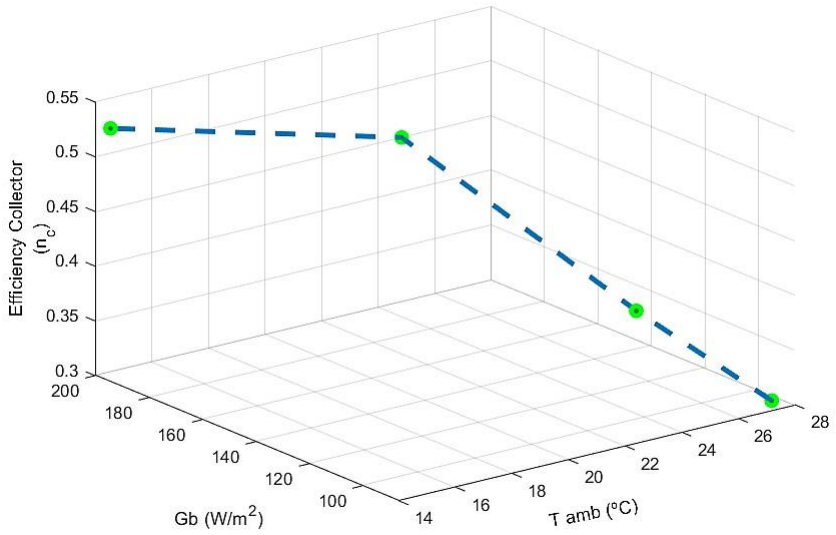

Figure 7. Collector efficiency vs ambient temperature and solar radiation.

Table 8. Collector performance based on the weather conditions of Ecuador.

Region	T_{amb} (°C)	G_b (W/m^2)	η_c
Coast	27.18	86.29	30.89%
Amazon	24.40	107.55	38.71%
Galapagos Islands	21.54	165.12	50.55%
Andean	14.07	194.98	53.06%

3.3. Energy storage tank analysis

Thermal based energy storage systems are more efficient and sustainable compared to traditional energy systems [50]. At almost any time, three zones coexist within the tank: A hot fluid zone at the top, a cold fluid zone at the bottom, and an intermediate zone called a transition [51]. In fact, the tank was divided into three main zones for modeling (hot-T_{s1}, transition-T_{s2}, and cold-T_{s3}), and its modeling was based on Eqs 4–6. As shown in Figure 8, T_{s1} corresponds to the inlet temperature to the ORC ($T_{oil,in}$), while T_{s3} corresponds to the inlet temperature to the solar collectors ($T_{c,in}$).

The analysis of the energy storage tank was conducted in a dynamic mode for a period of 168 h (7 days), using average temperature and solar radiation data recorded for the Sierra region (to maximize collector efficiency; see Section 3.2.3) by the NREL with 30-minute measurement intervals (time series 2012–2022).

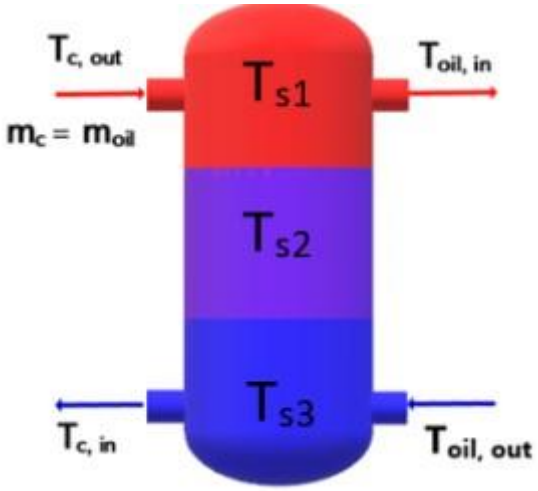

Figure 8. Energy storage tank (Temperatures).

Figure 9 illustrates the temperature variation in the hot zone over seven days of analysis. During this period, there was no significant variation in this zone, with a range of approximately 1.3 °C (from 293.19 to 291.95 °C). This suggests that once a steady state is achieved, the changes occurring in the hot zone are practically negligible. The temperature decrease occurs from 00:00 a.m. to 6:00 a.m., where no normal direct radiation data is recorded. Furthermore, an increase in the Tc is observed when the radiation levels rise during the day from 6:00 a.m. to 7:00 p.m. Subsequently, the same trend is observed throughout the 7-day analysis. The temperature drop is attributed to the thermodynamic properties of the thermal oil, which has a high specific heat, causing the last term in Eq 4 to be minimal, thus resulting in the dT_{s1}/dt evolution with time being virtually unaffected.

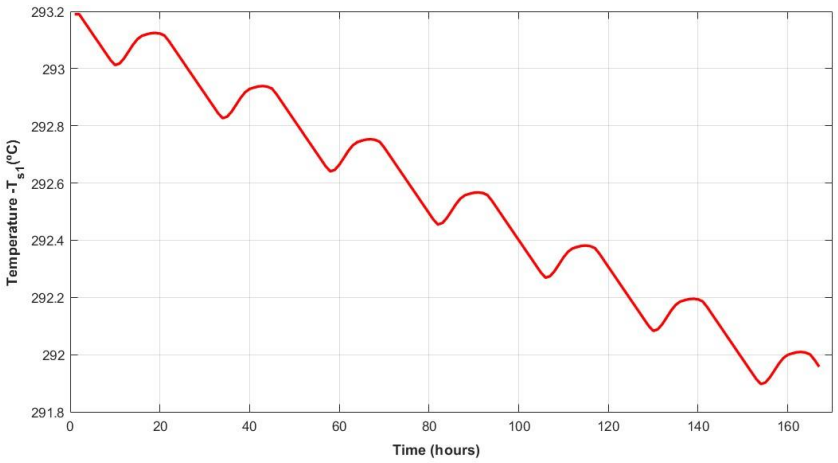

Figure 9. T_{s1} variation in the storage tank (hot zone).

On the other hand, the temperature of the transition zone (T_{s2}) is directly influenced by temperature variations in both the hot and cold zones (i.e., exchanging heat with both ends of the tank). As shown in Figure 10, the variation of T_{s2} follows a polynomial trend. However, similar to T_{s1}, the temperature change is minimal (<0.5 ℃), ranging from 276.5 to 276.36 ℃. This is because it receives heat from both the hot and cold zones, and both terms (T_{s1} and T_{s3}) in Eq 5 contribute to the temperature increase, with only the last term causing a decrease. As mentioned in the previous analysis, the thermodynamic properties of the thermal oil (specifically, density and C_p) are responsible for this term being so small.

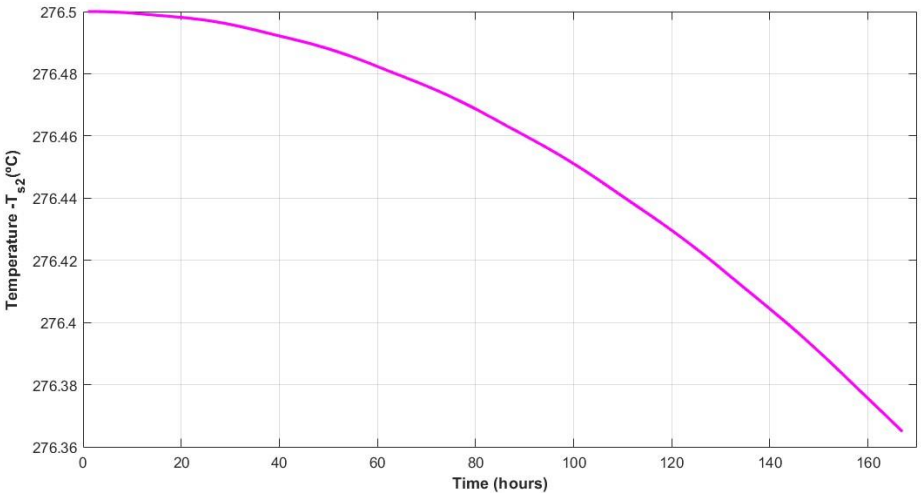

Figure 10. T_{s2} variation in the storage tank (Transition zone).

Finally, the temperature variation in the cold zone follows a linear trend with a negative slope (Figure 11). This zone undergoes more significant changes compared to the upper zones; however, similar to the upper zones, the change is minimal (<2.5 ℃), ranging from 259.83 to 257.39 ℃. This zone is directly dependent on the temperature of the oil at the Rankine organic cycle outlet, which, in turn, depends on the net heat required by the ORC. Despite being referred to as the cold zone, the

temperature difference between the hot and cold zones does not exceed 50 ℃, which is within the design range of the thermodynamic cycle. This temperature difference is due to the depth and volume of the tank. However, it is important to note that no significant thermoclines are formed, which allows for water stratification, where the colder and denser water moves towards the bottom and the warmer and less dense water moves towards the top, separated by a transition zone (thermocline).

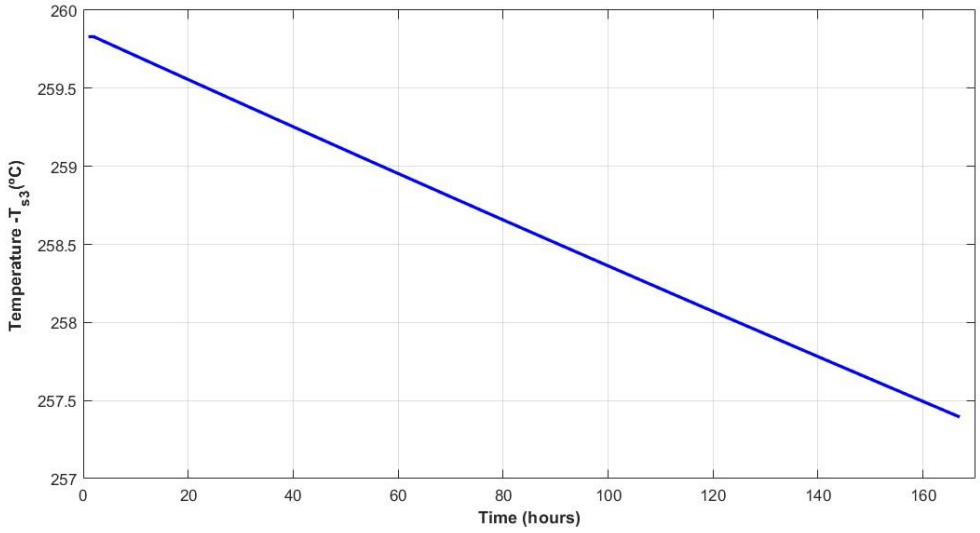

Figure 11. T_{s3} variation in the storage tank (Cold zone).

3.4. ORC analysis

3.4.1. Analysis of ORC performance based on the evaporation temperature of the working fluid prior to turbine inlet

To perform this analysis, the condensation temperature of the working fluids (60 ℃—Toluene and Water, 40 ℃—Cyclohexane, 87 ℃—Siloxane D4) was kept constant, and the evaporation temperature (i.e., the inlet temperature to the turbine) was varied within a range of 210 to 310 ℃, thus considering that it is an ORC operated at high temperatures and taking the critical temperatures of each fluid into account. As shown in Figure 12, for all working fluids except Siloxane D4, the ORC efficiency increases as the boiling temperature increases. The efficiency improvements for cyclohexane, toluene, and water are 2.72%, 2.05%, and 1.34%, respectively.

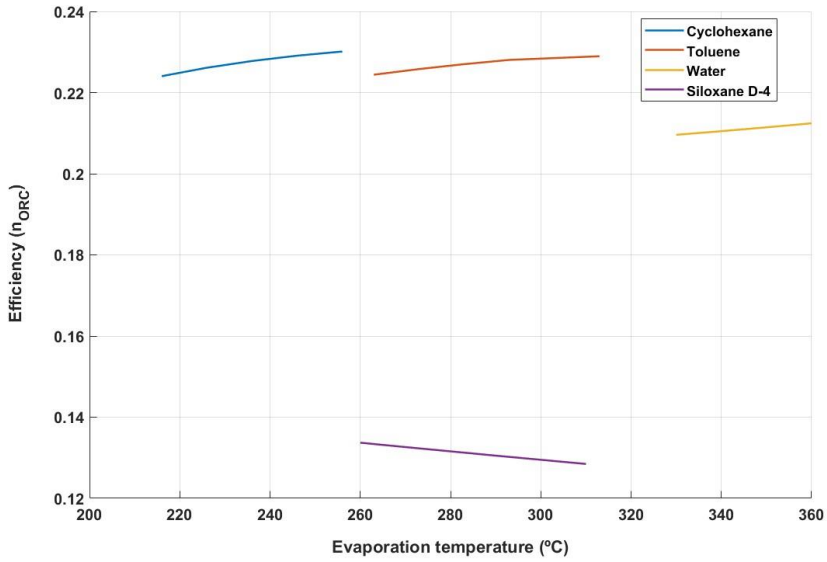

Figure 12. ORC efficiency vs evaporation temperature (°C).

3.4.2. Analysis of ORC performance based on the condensation temperature of the working fluid prior to the turbine inlet

To perform this analysis, the evaporation temperature of the working fluids (302 °C—Toluene, 265 °C—Cyclohexane, 307 °C—Siloxane D4) was kept constant, and the condensation temperature (i.e., the inlet temperature to the pump) was varied within a range of 30 to 110 °C. As shown in Figure 13, for all working fluids, the ORC efficiency decreases as the condensation temperature increases. The decrease in cycle efficiency for toluene, cyclohexane, and Siloxane D4 are 20.97%, 4.67%, and 16%, respectively.

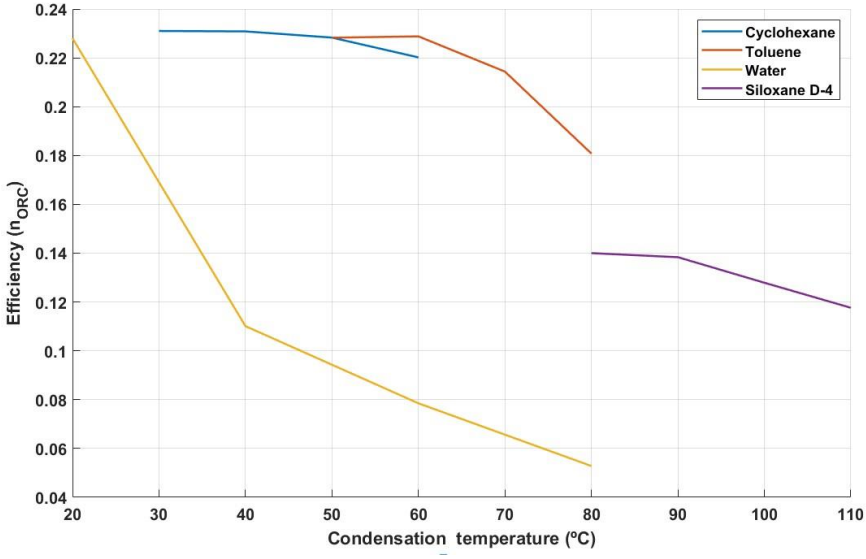

Figure 13. ORC efficiency vs condensation temperature (°C).

3.4.3. Analysis of the net work contribution provided by the ORC based on the pinch point temperature

According to the detailed results in Table 9, increasing the Pinch Point temperature (PP) leads to a decrease in the net work produced by the system. The choice of the PP temperature mainly depends on economic factors, since relatively low PP values increase the heat transfer area, thereby resulting in higher operating costs. Therefore, it is necessary to establish a minimum variation of the PP temperature to maximize the net work production while minimizing the operating costs of the system. Based on the results, cyclohexane produces the highest net work for the analyzed temperatures, thus leading to higher ORC efficiencies.

Table 9. Net work varying the pinch point (PP) temperature.

Working fluid	Parameter	PP temperature			
		0 ℃	10 ℃	20 ℃	30 ℃
Cyclohexane	W_{net}	-	-	379.73	230.61
Toluene		363.99	222.72	160.53	125.54
Water		132.99	111.47	95.97	84.27
Siloxane D4		101.24	78.61	64.27	54.37

Additionally, it can be observed in Table 9 that the W_{net} values are equal to zero for cyclohexane when the PP temperature is within the range of 0 to 10 ℃. The ORC does not function properly when the temperature gradient between the thermal oil and the ORC fluid is limited. This temperature gradient facilitates the heat transfer between fluids and the generation of W_{net}. The thermodynamic properties of cyclohexane contribute to this limitation, including its notably low critical temperature compared to other fluids tested (280.5 ℃).

3.5. Analysis of the thermal module—ORC

3.5.1. Analysis of the total system performance based on heat transfer area and thermal storage tank volume

Figure 14 indicates that for the same operating conditions, the working fluid that yields the best total system efficiencies is cyclohexane, thus reaching a maximum efficiency of approximately 25.13% under the most favorable conditions. In contrast, toluene, water, and siloxane D4 show efficiencies of 22%, 20.61%, and 14.99%, respectively.

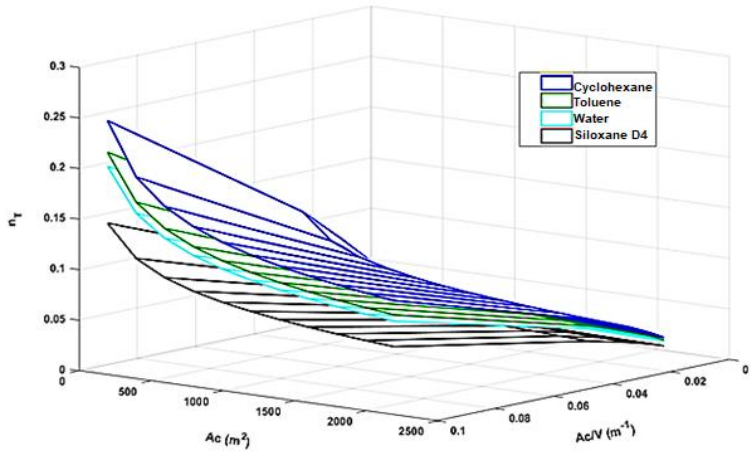

Figure 14. Total system efficiency as a function of area and Ac/V ratio of the collector Wnom = f (Collector area).

3.5.2. Analysis of the net system work by adding a waste heat source to the ORC

The addition of waste heat to an ORC constitutes a cogeneration system, which involves harnessing exhaust gases from an industrial process (typically in cement, sugar, or ceramic industries), where waste heat is generated in the range of 10 kW to 10 MW [52]. Figure 15 schematizes the ORC powered by waste heat and solar energy. As seen in Figure 16, when an extra heat source is added ((Q_w) = 184 kW, temperature level: 250 °C), W_{net} increases significantly compared to the W_{net} produced when the system operates solely using solar collectors as the energy source. The net work without waste heat added to the system is 18.30 kW. However, when waste heat is added, it increases to 65.09 kW. This means an approximate increase of 255%.

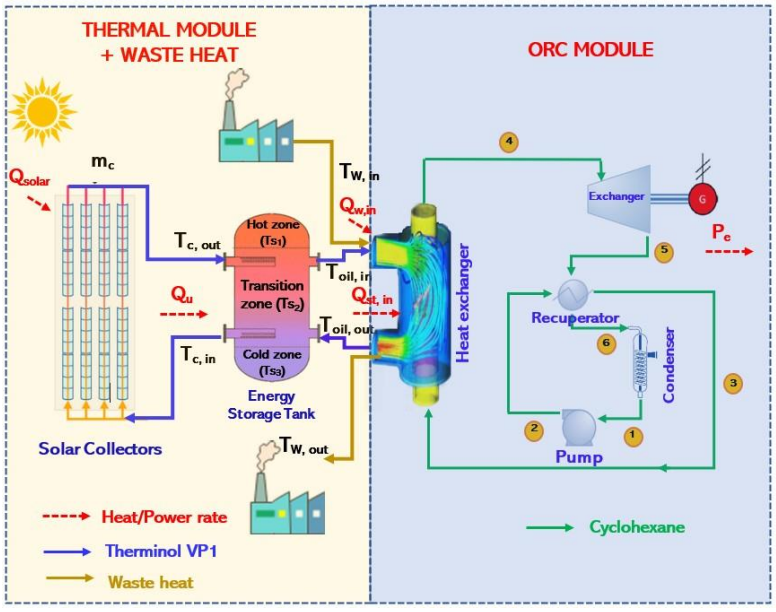

Figure 15. ORC integrated with waste heat and solar collectors.

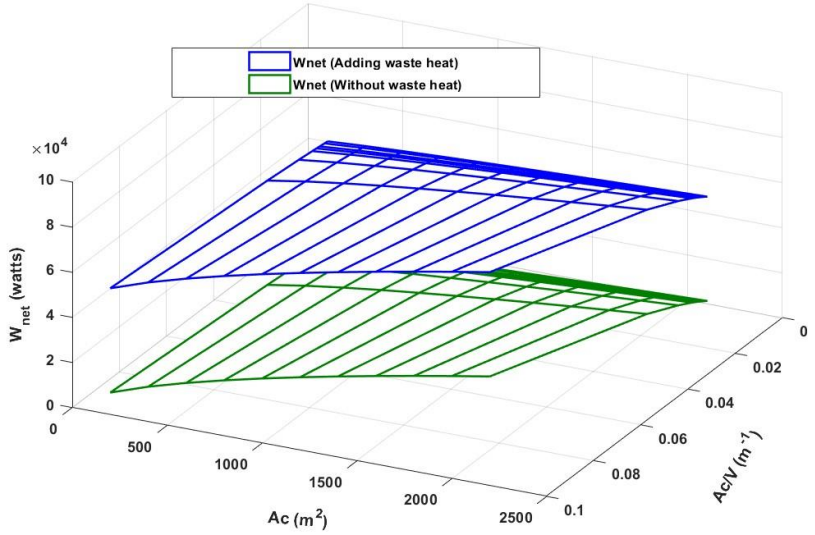

Figure 16. Net work only with solar collectors and adding a waste heat source.

3.5.3. Analysis of the internal rate of return (*IRR*)

The analysis of the IRR is widely regarded as a crucial assessment within the realm of economics due to its ability to ascertain the viability of a given project. When conducting this analysis, cyclohexane is employed as the designated working fluid. For the financial analysis, energy cogeneration has been considered, adding an extra source of energy (i.e., waste heat) to increase the profitability of the system. The discount factor (r) which makes the NPV equal to zero (Eq 16) is equal to the IRR of the investment.

As observed in Figure 17a, the *IRR* increases as the collector area increases; however, this increase reaches a maximum peak (*IRR* = 15.66%) when the collector area is in the range of 1400 to 1650 m^2. Beyond this value, the *IRR* starts to decline. This effect occurs because the system has been designed to work with a maximal nominal power of 92 kW. Once the collector area reaches 1600 m^2, the capacity factor becomes 100%, and further increasing the solar collector area does not significantly contribute to the net work output of the system. Moreover, the initial investment costs exponentially increase with the expansion of the solar capture area, thus leading to a decrease in the growth curve.

Similarly, in Figure 17b, it can be observed that the *IRR* remains nearly constant as the *A*c/V ratio increases. However, a maximum peak is also observed when the ratio falls within the range of 0.02 to 0.04 m^{-1}. According to the optimization of the system, the optimal collector area is 1600 m^2 with an *A*c/*V* ratio of (1/30) m^{-1}.

Once the maximum rate of return is determined, it is important to identify the minimum payback period to recover the investment and start realizing profits. The payback period corresponds to the number of years for which the Net Present Value (NPV) is minimized. Based on Figure 18, the payback period for the implementation of the system is 9.81 years.

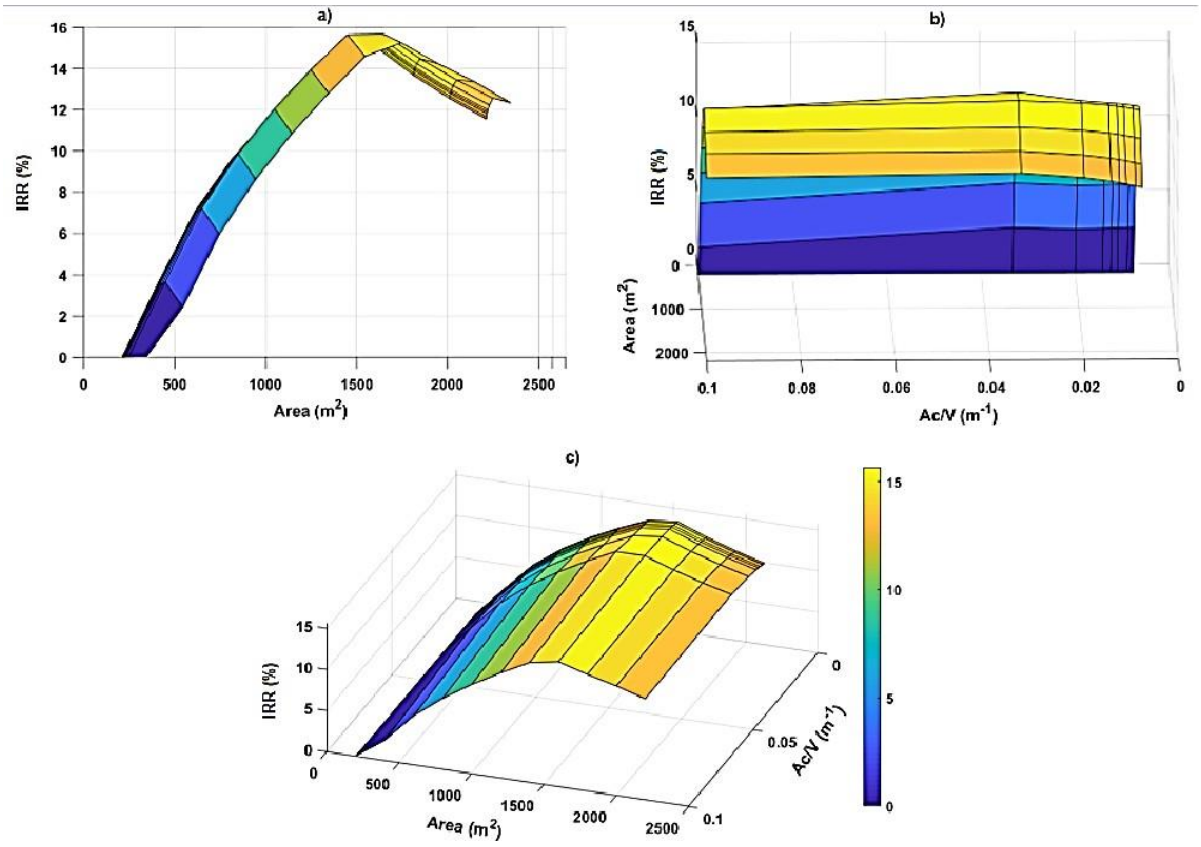

Figure 17. (a) Internal rate of return (*IRR*) as a function of the collector area; (b) *IRR* as a function of *A*c/*V* ratio; (c) *IRR* as a function of both the collector area and the *A*c/*V* ratio.

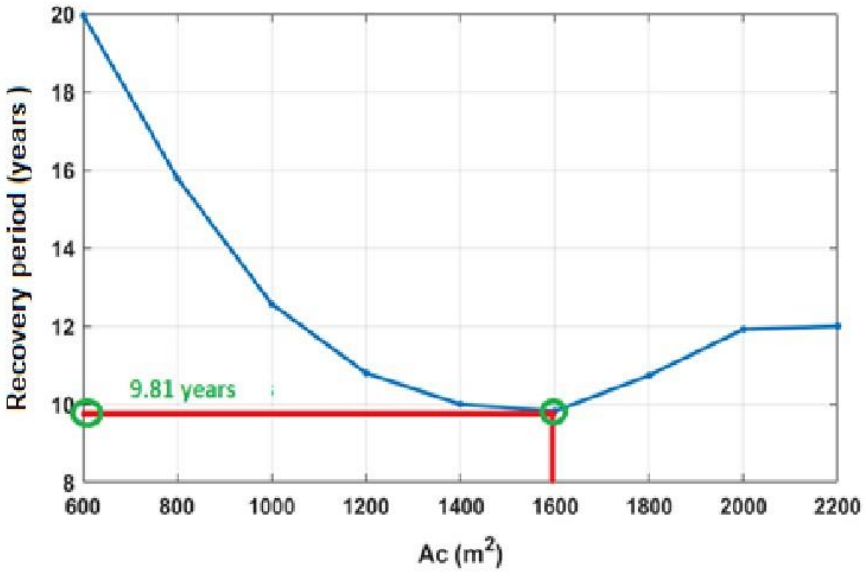

Figure 18. Recovery period with respect to the initial investment (*A*c/*V* = 30 m^{-1}).

3.6. *Optimal operating conditions*

The system optimization was conducted using the average temperature and solar radiation data collected at 30-minute intervals from the 2012–2022 time series, in combination with the financial parameters detailed in Table 4. It's worth noting that the model is adaptable, thereby enabling modifications to accommodate evolving climatic conditions and financial parameters in future research.

Finally, Table 10 summarizes the results for the optimal operating conditions using Therminol VP1 as the thermal fluid and cyclohexane as the organic working fluid for the ORC. The conditions are based on the meteorological conditions of the Andean Region in Ecuador, and the values of Ac and Ac/V ratio are chosen to maximize the *IRR* and minimize the recovery period.

Table 10. Optimal operating conditions.

Parameter	Unit	Value	Parameter	Unit	Value
Collector area (Ac)	m^2	1600	*IRR*	%	15.65
Energy storage volume(V)	m^3	54	Recovery period	years	9.81
Oil inlet temperature ($T_{oil,in}$)	℃	292.34	Electric energy per year	MW	23757
Collector efficiency (η_c)	%	50.42%			
ORC efficiency (n_T)	%	25.01%			
System efficiency (n_T)	%	20.86%			

4. Conclusions

A mathematical modeling of an ORC operated with solar collectors was conducted to evaluate the performance of the thermal module and the ORC by analyzing various operational parameters. The thermal module was tested with four thermal fluids: Therminol VP1, Hitec, molten salts, and Hitec XL. The solar collectors achieved the highest efficiency (55.40%) when using Therminol VP1 as the thermal fluid. The efficiency of the collectors under different meteorological conditions (pressure and temperature) in each region of Ecuador was as follows: 53.06% in the Andean region, 50.55% in the Galapagos Island region, 38.71% in the Amazon region, and 30.89% in the Coast region. Therefore, it is suggested that implementing a system of this type would be more viable in the Andean and Galapagos regions.

On the other hand, based on the analysis, it was determined that the ORC's efficiency decreases with an increase in the condensation temperature, as it indirectly raises the condensation pressure and the actual work of the pump. Regarding the evaporation temperature, the ORC's efficiency is proportional: higher temperatures lead to increased turbine work. However, the temperature cannot exceed the critical temperature of each fluid, beyond which it becomes unstable.

Furthermore, the ORC' s efficiency increases with the collector's area, and the same effect applies to the Ac/V ratio. For Ac/V = 130^{-1}, with Ac = 200 m^2, the net work (W_{net}) performed is 1.45 kW; if the Ac increases tenfold (2000 m^2), the W_{net} rises to 6.74 kW. Meanwhile, if the Ac/V ratio increases to 10^{-1}, the W_{net} at Ac = 200 m^2 considerably increases to 37.03 kW. However, higher Ac and Ac/V ratios result in a larger energy storage tank volume and increased system implementation costs.

Cyclohexane is the organic fluid that best suits the system's operation, thereby leading to the highest ORC efficiency. When adding waste heat, the increase in electricity production rate significantly rises when using cyclohexane, reaching up to 255% in production. This percentage varies

depending on the collector's area. Under optimal operating conditions, the net work produced increased from 18.30 to 65.09 kW.

Finally, the system was optimized, resulting in an IRR equivalent to 15.65%, with a payback period of 9.81 years. These results were obtained with a total collector area of 1600 m^2 and an energy storage tank volume of 54 m^3. The estimated electricity production is 23757 MW per year, with collector efficiency, ORC efficiency, and overall system efficiency at 50.42%, 25.01%, and 20.86%, respectively.

In the context of future work and further research, it is imperative to advance our modeling approach by optimizing it under dynamic conditions. This will involve the incorporation of meteorological conditions that are in line with the evolving global climate patterns. Additionally, we plan to implement more sophisticated collector tracking methods to enhance the accuracy of our model. These improvements will enable us to account for the dynamic nature of solar energy generation, thereby ensuring that our system operates efficiently and effectively under changing environmental conditions.

Use of AI tools declaration

The authors declare they have not used Artificial Intelligence (AI) tools in the creation of this article.

Acknowledgments

The authors thank the Security Research Group on Environment and Engineering, "GISAI" for allowing the execution of this research.

Conflict of interest

The authors declare no conflict of interest.

References

1. Davidy A (2021) Thermodynamic design of Organic Rankine Cycle (ORC) based on petroleum coke combustion. *ChemEngineering* 5: 37. https://doi.org/10.3390/chemengineering5030037
2. ARCONEL, *National Electrical Energy Balance—Photovoltaic Energy Production*. Available from: https://www.controlrecursosyenergia.gob.ec/balance-nacional-de-energia-electrica/.
3. Qu D, Cheng L, Bao Y, et al. (2022) Enhanced optical absorption and solar steam generation of CB-ATO hybrid nanofluids. *Renewable Energy* 199: 509–516. https://doi.org/10.1016/j.renene.2022.08.150
4. Bao Y, Huang A, Zheng X, et al. (2023) Enhanced photothermal conversion performance of MWCNT/SiC hybrid aqueous nanofluids in direct absorption solar collectors. *J Mol Liq* 387: 122577. https://doi.org/10.1016/j.molliq.2023.122577
5. Ministry of Electricity and Renewable Energy (2017) *National Energy Efficiency Plan 2016–2035*. Available from: https://www.acreditacion.gob.ec/sae-en-el-plan-de-eficiencia-energetica-2016-2035/.
6. Hung TC, Shai TY, Wang SK (1997) A review of Organic Rankine Cycles (ORCs) for the recovery of low-grade waste heat. *Energy* 22: 661–667. https://doi.org/10.1016/S0360-5442(96)00165-X

7. Bao J, Zhao L (2013) A review of working fluid and expander selections for Organic Rankine Cycle. *Renewable Sustainable Energy Rev* 24: 325–342. https://doi.org/10.1016/j.rser.2013.03.040
8. Lecompte S, Huisseune H, Van Den Broek M, et al. (2015) Review of Organic Rankine Cycle (ORC) architectures for waste heat recovery. *Renewable Sustainable Energy Rev* 47: 448–461. https://doi.org/10.1016/j.rser.2015.03.089
9. Vélez F, Segovia JJ, Martín MC, et al. (2012) A technical, economical and market review of Organic Rankine Cycles for the conversion of low-grade heat for power generation. *Renewable Sustainable Energy Rev* 16: 4175–4189. https://doi.org/10.1016/j.rser.2012.03.022
10. Zhai H, An Q, Shi L, et al. (2016) Categorization and analysis of heat sources for Organic Rankine Cycle systems. *Renewable Sustainable Energy Rev* 64: 790–805. https://doi.org/10.1016/j.rser.2016.06.076
11. Karellas S, Leontaritis AD, Panousis G, et al. (2013) Energetic and exergetic analysis of waste heat recovery systems in the cement industry. *Energy* 58: 147–156. https://doi.org/10.1016/j.energy.2013.03.097
12. Tzivanidis C, Bellos E, Antonopoulos KA (2016) Energetic and financial investigation of a stand-alone solar-thermal Organic Rankine Cycle power plant. *Energy Convers Manage* 126: 421–433. https://doi.org/10.1016/j.enconman.2016.08.033
13. Delgado-Torres AM, García-Rodríguez L (2012) Design recommendations for solar Organic Rankine Cycle (ORC)—Powered reverse osmosis (RO) desalination. *Renewable Sustainable Energy Rev* 16: 44–53. https://doi.org/10.1016/j.rser.2011.07.135
14. Ferrara F, Gimelli A, Luongo A (2014) Small-scale concentrated solar power (CSP) plant: ORCs comparison for different organic fluids. *Energy Procedia* 45: 217–226. https://doi.org/10.1016/j.egypro.2014.01.024
15. Bianchi M, De Pascale A (2011) Bottoming cycles for electric energy generation: Parametric investigation of available and innovative solutions for the exploitation of low and medium temperature heat sources. *Appl Energy* 88: 1500–1509. https://doi.org/10.1016/j.apenergy.2010.11.013
16. Sampedro Redondo JL (2017) Application of low-temperature Organic Rankine Cycles to microgeneration systems. University of Oviedo. Available from: http://hdl.handle.net/10651/44967.
17. Borsukiewicz-Gozdur A, Nowak W (2007) Comparative analysis of natural and synthetic refrigerants in application to low temperature Clausius-Rankine cycle. *Energy* 32: 344–352. https://doi.org/10.1016/j.energy.2006.07.012
18. Schuster A, Karellas S, Kakaras E, et al. (2009) Energetic and economic investigation of Organic Rankine Cycle applications. *Appl Therm Eng* 29: 1809–1817. https://doi.org/10.1016/j.applthermaleng.2008.08.016
19. Chacartegui R, Vigna L, Becerra JA, et al. (2016) Analysis of two heat storage integrations for an Organic Rankine Cycle Parabolic trough solar power plant. *Energy Convers Manage* 125: 353–367. https://doi.org/10.1016/j.enconman.2016.03.067
20. Chen Y, Pridasawas W, Lundqvist P (2007) Low-grade heat source utilization by carbon dioxide transcritical power cycle. *Heat Transfer Summer Conf* 42746: 519–525. https://doi.org/10.1115/HT2007-32774

21. Kaneko S (2016) Integrated coal gasification combined cycle: A reality, not a dream. *J Energy Eng* 142: E4015018. https://doi.org/10.1061/(ASCE)EY.1943-7897.0000312
22. Wang XD, Zhao L, Wang JL, et al. (2010) Performance evaluation of a low-temperature solar Rankine cycle system utilizing R245fa. *Sol Energy* 84: 353–364. https://doi.org/10.1016/j.solener.2009.11.004
23. Bellos E, Tzivanidis C, Antonopoulos KA (2016) Exergetic, energetic and financial evaluation of a solar driven absorption cooling system with various collector types. *Appl Therm Eng* 102: 749–759. https://doi.org/10.1016/j.applthermaleng.2016.04.032
24. Bišćan D, Filipan V (2012) Potential of waste heat in Croatian industrial sector. *Therm Sci* 16: 747–758. https://doi.org/10.2298/TSCI120124123B
25. Tchanche BF, Lambrinos G, Frangoudakis A, et al. (2011) Low-grade heat conversion into power using Organic Rankine Cycles—A review of various applications. *Renewable Sustainable Energy Rev* 15: 3963–3979. https://doi.org/10.1016/j.rser.2011.07.024
26. Sprouse III C, Depcik C (2013) Review of Organic Rankine Cycles for internal combustion engine exhaust waste heat recovery. *Appl Therm Eng* 51: 711–722. https://doi.org/10.1016/j.applthermaleng.2012.10.017
27. Xie H, Yang C (2013) Dynamic behavior of Rankine cycle system for waste heat recovery of heavy duty diesel engines under driving cycle. *Appl Energy* 112: 130–141. https://doi.org/10.1016/j.apenergy.2013.05.071
28. Zhang HG, Wang EH, Fan BY (2013) A performance analysis of a novel system of a dual loop bottoming Organic Rankine Cycle (ORC) with a light-duty diesel engine. *Appl Energy* 102: 1504–1513. https://doi.org/10.1016/j.apenergy.2012.09.018
29. Franco A, Villani M (2009) Optimal design of binary cycle power plants for water-dominated, medium-temperature geothermal fields. *Geothermics* 38: 379–391. https://doi.org/10.1016/j.geothermics.2009.08.001
30. Zhai H, Shi L, An Q (2014) Influence of working fluid properties on system performance and screen evaluation indicators for geothermal ORC (Organic Rankine Cycle) system. *Energy* 74: 2–11. https://doi.org/10.1016/j.energy.2013.12.030
31. García-Rodríguez L, Blanco-Gálvez J (2007) Solar-heated Rankine cycles for water and electricity production : POWERSOL project. *Desalination* 212: 311–318. https://doi.org/10.1016/j.desal.2006.08.015
32. Algieri A, Morrone P (2014) Energetic analysis of biomass-fired ORC systems for micro-scale combined heat and power (CHP) generation. A possible application to the Italian residential sector. *Appl Therm Eng* 71: 751–759. https://doi.org/10.1016/j.applthermaleng.2013.11.024
33. Algieri A, Morrone P (2014) Techno-economic analysis of biomass-fired ORC systems for single-family combined heat and power (CHP) applications. *Energy Procedia* 45: 1285–1294. https://doi.org/10.1016/j.egypro.2014.01.134
34. Drescher U, Brüggemann D (2007) Fluid selection for the Organic Rankine Cycle (ORC) in biomass power and heat plants. *Appl Therm Eng* 27: 223–228. https://doi.org/10.1016/j.applthermaleng.2006.04.024
35. Naranjo-Silva S, Punina-Guerrero D, Rivera-Gonzalez L, et al. (2023) Hydropower scenarios in the face of climate change in Ecuador. *Sustainability* 15: 10160. https://doi.org/10.3390/su151310160

36. Kalogirou SA (2004) Solar thermal collectors and applications. *Prog Energy Combust Sci* 30: 231–295. https://doi.org/10.1016/j.pecs.2004.02.001
37. Tzivanidis C, Bellos E, Antonopoulos KA (2016) Energetic and financial investigation of a stand-alone solar-thermal Organic Rankine Cycle power plant. *Energy Convers Manage* 126: 421–433. https://doi.org/10.1016/j.enconman.2016.08.033
38. Bellos E, Tzivanidis C (2020) Parametric investigation of a trigeneration system with an Organic Rankine Cycle and absorption heat pump driven by parabolic trough collectors for the building sector. *Energies* 13: 1800. https://doi.org/10.3390/en13071800
39. Cabrera FJ, Fernández-García A, Silva RMP, et al. (2013) Use of parabolic trough solar collectors for solar refrigeration and air-conditioning applications. *Renewable Sustainable Energy Rev* 20: 103–118. https://doi.org/10.1016/j.rser.2012.11.081
40. Pei G, Li J, Ji J (2010) Analysis of low temperature solar thermal electric generation using regenerative Organic Rankine Cycle. *Appl Therm Eng* 30: 998–1004. https://doi.org/10.1016/j.applthermaleng.2010.01.011
41. Sadeghi M, Nemati A, Yari M (2016) Thermodynamic analysis and multi-objective optimization of various ORC (Organic Rankine Cycle) configurations using zeotropic mixtures. *Energy* 109: 791–802. https://doi.org/10.1016/j.energy.2016.05.022
42. Wang R, Jiang L, Ma Z, et al. (2019) Comparative analysis of small-scale Organic Rankine Cycle systems for solar energy utilisation. *Energies* 12: 829. https://doi.org/10.3390/en12050829
43. Cao Y, Gao Y, Zheng Y, et al. (2016) Optimum design and thermodynamic analysis of a gas turbine and ORC combined cycle with recuperators. *Energy Convers Manage* 116: 32–41. https://doi.org/10.1016/j.enconman.2016.02.073
44. Yu H, Helland H, Yu X, et al. (2021) Optimal design and operation of an Organic Rankine Cycle (ORC) system driven by solar energy with sensible thermal energy storage. *Energy Convers Manage* 244: 114494. https://doi.org/10.1016/j.enconman.2021.114494
45. Karim SHT, Tofiq TA, Shariati M, et al. (2021) 4E analyses and multi-objective optimization of a solar-based combined cooling, heating, and power system for residential applications. *Energy Rep* 7: 1780–1797. https://doi.org/10.1016/j.egyr.2021.03.020
46. Ochoa GV, Ortiz EV, Forero JD (2023) Thermo-economic and environmental optimization using PSO of solar Organic Rankine Cycle with flat plate solar collector. *Heliyon* 9: e13697. https://doi.org/10.1016/j.heliyon.2023.e13697
47. Alshammari S, Kadam ST, Yu Z (2023) Assessment of single rotor expander-compressor device in combined Organic Rankine Cycle (ORC) and vapor compression refrigeration cycle (VCR). *Energy* 282: 128763. https://doi.org/10.1016/j.energy.2023.128763
48. Maccari A, Bissi D, Casubolo G, et al. (2015) Archimede solar energy molten salt parabolic trough demo plant: A step ahead towards the new krontiers of CSP. *Energy Procedia* 69: 1643–1651. https://doi.org/10.1016/j.egypro.2015.03.122
49. Krishna Y, Faizal M, Saidur R, et al. (2020) State-of-the-art heat transfer fluids for parabolic trough collector. *Int J Heat Mass Transfer* 152: 119541. https://doi.org/10.1016/j.ijheatmasstransfer.2020.119541
50. Işık S, Yıldız C (2020) Improving thermal energy storage efficiency of solar collector tanks by placing phase change materials in novel finned-type cells. *Therm Sci Eng Prog* 19: 100618. https://doi.org/10.1016/j.tsep.2020.100618

51. Fasquelle T, Falcoz Q, Neveu P, et al. (2017) Operating results of a thermocline thermal energy storage included in a parabolic trough mini power plant. *AIP Conf Proc* 1850. https://doi.org/10.1063/1.4984431
52. Haunreiter Echeverría B (2017) Study of technical and economic alternatives for the recovery of waste heat at the Quevedo II thermoelectric plant, taking into account climate change mitigation aspects. Available from: http://bibdigital.epn.edu.ec/handle/15000/17498.

AIMS Press